MANUFACTURING AND MECHANICAL & METALLURGICAL PROPERTIES OF 9 ~ 12%CR ROTOR FORGINGS STEEL FOR ADVANCED STEAM TURBINE

Sung-Tae Kang, Dong-Su Kim, Kul-Cheol Kim, Min-Su Kim, Seog-Heyon Ryu and Jeong-Tae Kim – Doosan Heavy Industries Co., Ltd., Korea

ABSTRACT

A thermal efficiency improvement of the power plant does reduce the fuel costs as well as SOx, NOx and CO_2 emission. In order to be used in these advanced operating conditions, the economic ferrite steels with creep resistance are required for highly stressed turbine components. In the frame of the European research activities COST 501/522, tungsten added 9 ~ 12%Cr steels have developed and used for turbine applications.

This paper deals with the experiences in manufacturing and ultrasonic testing, the mechanical and metallurgical properties of the tungsten added 10%Cr steel for high and intermediate pressure(HIP) rotor forgings. The creep behaviour and fatigue crack resistance of the tungsten added 10%Cr steel were superior to those of the conventional 12%Cr steel. The microstructures responsible for superior creep rupture strength and fatigue characteristics are described and discussed in this paper.

KEYWORDS

HIP ROTOR FORGING, 9~12%CR STEEL, CREEP RUPTURE STRENGTH, FACTIGUE AND EELECRO SLAG REMELTING

INTRODUCTION

It has been a trend that the steam temperature of steam turbine is pushed being higher and higher to improve thermal efficiency. This means that the materials for such as HIP rotor are required to withstand the higher temperature. The concerning properties in rotor design and its operation are same to those relating to the structural integrity of rotor operating under stress conditions and temperature for the machine life. Rotors must have a high resistance to the crack initiation and its propagation under low/high cycle loading. And also rotors have high creep resistance under long time exposure in steady state stress at elevated temperature and in brittle fracture at low nominal temperature.

A lot of efforts have been made to develop new ferritic heat resistant steels for thermal power plants operated at advanced steam conditions since 1990s. However, the steels to meet the requirements for the application above 621^{o}C have not been realized.

Many researchers reported that the addition of W and/or Mo had beneficial effects on the long-term creep rupture strength [1-5] in 9-12%Cr heat resistant steels. The addition of tungsten (W) and molybdenum(Mo) strengthened the matrix due to the solution hardening and precipitates after final heat treatments, high toughness and creep strength could be obtained. It is characteristics of all the tungsten alloyed steels more than 1.7% W that they feature relatively high creep strength below

HOME

10000 hrs which, however, declines in the long term range. This reduction is less pronounced in case of 9~12%Cr steels with approximately 1.5 Mo equivalent[6, 7]. Commercial materials like TOS107[8] and COST E [9] generally contained 1% W content.

There is a joint development program for the partners consisting of boiler and turbine manufacturers, steelworks, power utilities and research institutes in Korea. Under this program, 9 ~ 12%Cr steels for using up to 600°C were considered, trial rotor forgings with body diameters in 1100 mm were manufactured. Effects of alloying elements on the mechanical and metallurgical properties of these materials had reported in several papers[10-12].

This paper describes the development and manufacturing of 12%Cr steels for 600°C class steam turbine rotor. The purpose of this study was to obtain 12%Cr martensitic steel with high creep rupture strength and low notched susceptibility at elevated temperature. The applicable target of this steel is the high and intermediate pressure rotor forgings of thermal power plants of 600°C class. The target properties of this steel were as follows.

- 10^5h Creep rupture strength of about 100MPa at design temperature
- Creep rupture ductility more than 10% elongation
- Minimum yield strength of 700MPa

FUNDAMENTAL STUDY

The chemical compositions of steel used in this fundamental study are shown in Table 1. Alloy A is the conventional 12%Cr rotor steel developed from GE Company. Alloy B and C are the candidates of 600°C class rotor steel. Alloy B is a modified steel on the basis of the alloy A by adjusting carbon and molybdenum(Mo) contents. Alloy C has the similar chemical composition to that developed under the European COST 501 program(COST E). Because high creep rupture strength was obtained by increasing Mo and W contents and by prevention against delta ferrite, molybdenum and tungsten contents were determined as the molybdenum equivalent of about 1.5. The molybdenum equivalent was given as Mo + 1/2W(mass%).

All of the ingots were prepared by 1 ton vacuum induction melting and were forged into diameter 110 mm electrode in size. This steel was refined by the electro slag remelting(ESR) process to ensure a uniform chemical composition throughout the entire forgings. The steels were quenched at 1050°C and were tempered at 550 ~ 700°C. Mechanical properties such as tensile, creep rupture, low cycle fatigue(LCF) and high cycle fatigue(HCF) were evaluated. The microstructure was examined as tempered and crept state by optical microscope and transmission electron microscope(TEM). The type of carbide phases was analyzed by means of X-ray deffractometer.

Table 1 Chemical composition(%).

	C	Mn	Si	Ni	Cr	Mo	V	Nb	N	W
Alloy A	0.19	0.50	0.30	0.50	10.50	**1.0**	0.20	0.08	0.06	-
Alloy B	0.14	0.50	0.05	0.60	10.40	**1.5**	0.20	0.06	0.05	-
Alloy C	0.13	0.45	0.06	0.70	10.50	**1.0**	0.19	0.05	0.06	**1.0**

FUNDAMENTAL RESULTS

Alloy A refers to the HIP rotor forgings used from several tens years ago, while the others are the materials modified with Mo and W on the basis of alloy A. Mechanical properties such as tensile and creep rupture strength were evaluated to select optimum alloy. Yield strengths as the function of test temperature of alloy A, B and C are shown in Fig. 1. The 0.2% off-set yield strengths as the function of temperature of all alloys are very similar one another.

The creep rupture strengths against temperature were different in absolute values. Fig.2 shows the creep rupture strength as the function of rupture time for each alloy in terms of 600°C, 650°C and 704°C. The creep rupture strength at 600°C of alloy C is superior to those of alloy A and B up to about 3,000 hours as shown in Fig.2. Creep rupture strength at 650°C of alloy B and C converged to similar values. At a high applied stress, creep rupture strength at 704°C of alloy C was slightly lower than that of alloy B. However, at a lower applied stress, creep rupture strengths of both alloys would be crossed over after 100hr creep. The creep rupture strengths at all test temperatures of alloy C were superior to the other alloys. It is considered that the improvement of creep rupture strength resulted from the effects of tungsten on the solution hardening and the formation of fine Laves phase.

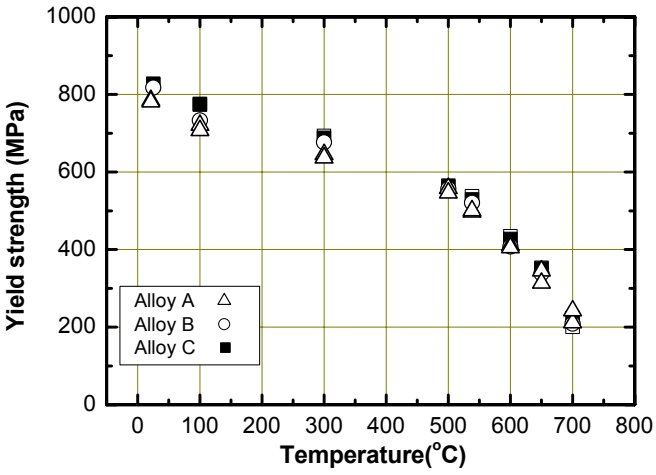

Fig. 1 Yield strengths with temperature of alloy A, B and C.

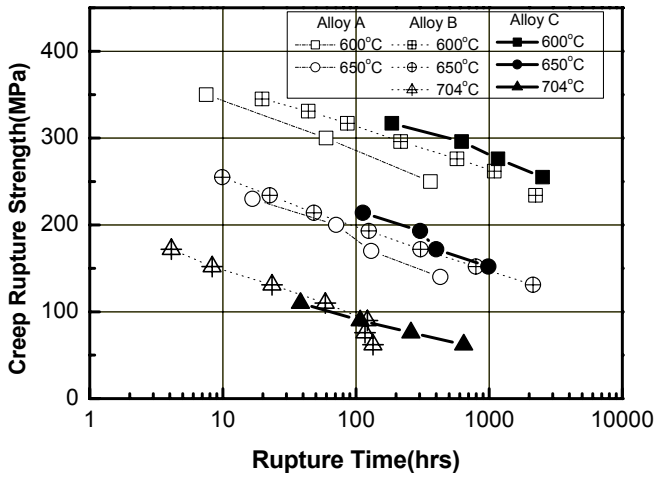

Fig. 2 Comparison of creep rupture strengths at 600°C, 650°C, and 704°C in alloy A, B and

Fig. 3 shows LCF results at room temperature for alloy A, B and C steels. For high strain amplitude, fatigue life is similar to each other, but fatigue characteristics at low strain amplitude of alloy C are superior to alloy A. The fatigue characteristics of alloy B and C are similar. The fatigue life and the striation width at the total strain range of 0.8% of alloy C are 21,800 cycles and 2.89 μm, respectively, as shown in Fig. 3 b). Small striation width indicates that the crack propagation length per cyclic loading after crack initiation is small. It has been known that the material with excellent resistance for crack initiation has good resistance for crack propagation.

HOME

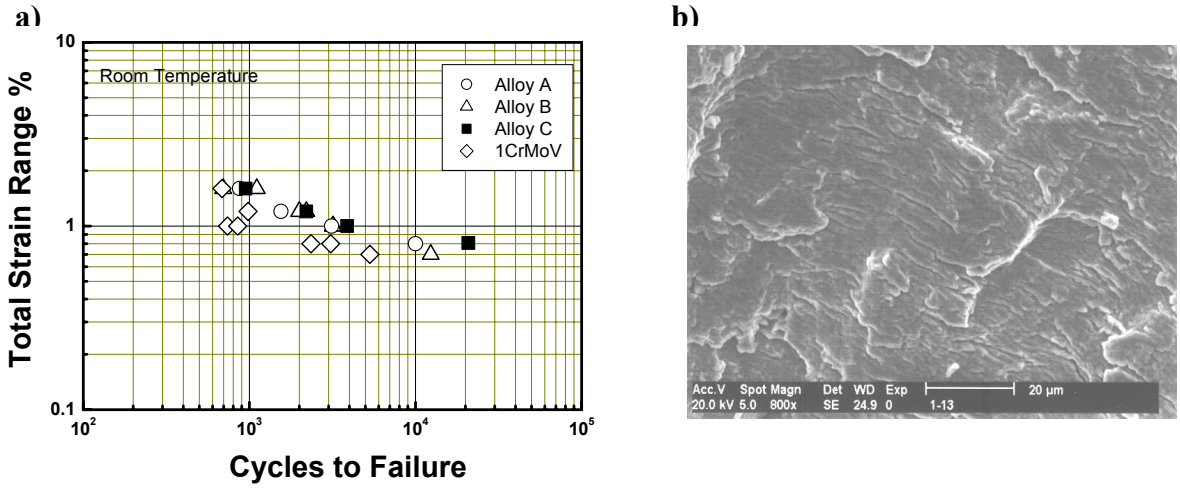

Fig. 3 Low cycle fatigue life of each alloy and fractograph at room temperature.
a) LCF life diagram for each alloys
b) Fractograph for alloy C($\Delta\varepsilon_T$ = 0.8%)

Fig. 4 shows HCF results for alloy A, B and C steels at 350°C temperature under zero mean stress condition. Alloy B and C are superior to alloy A. However, the HCF lives of both steels are almost same as shown in Fig. 4. In general, the higher creep rupture strength, the superior HCF characterics. The reason for more excellent HCF characterics of alloy B and C is the higher creep strength than that of alloy A. It seems that the higher fatigue life of alloy C is attributed by the hardening induced by fine precipitates and matrix solution strengthening by W addition.

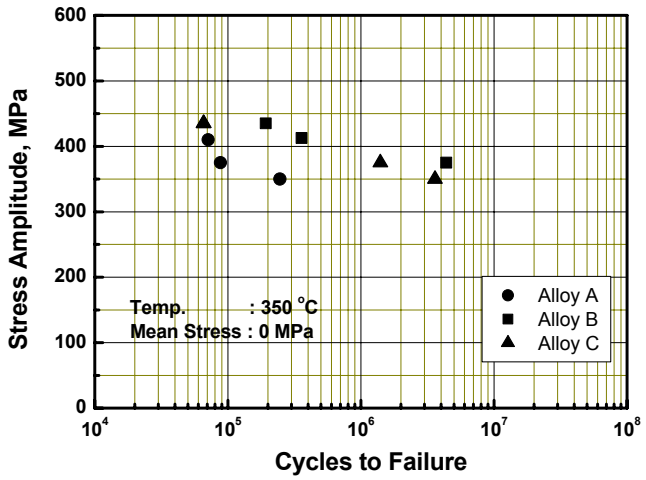

Fig. 4 High cycle fatigue life of each alloy at 350°C.

Microstructure changes as tempered and crept state were observed using the optical microscope. Delta-ferrite and segregated structures are not observed and microstructures as tempered state are typical tempered martensitic structure as shown in Fig.5. Fig. 6 shows optical micrographs for each alloy after crept. It was difficult to distinguish microstructure difference through optical microscope. However, it still reveals the tempered martensitic structure as shown in Fig. 6.

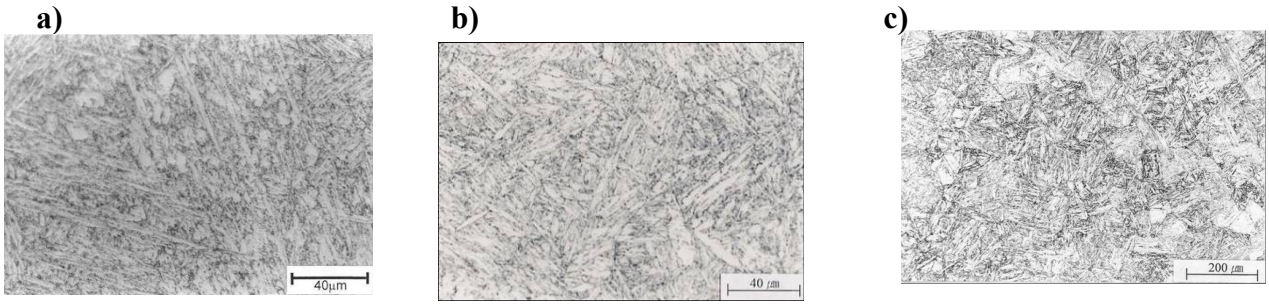

Fig.5 Comparison of the optical micrographs after oil quenching and double tempering.
a) Alloy A b) Alloy B c) Alloy C

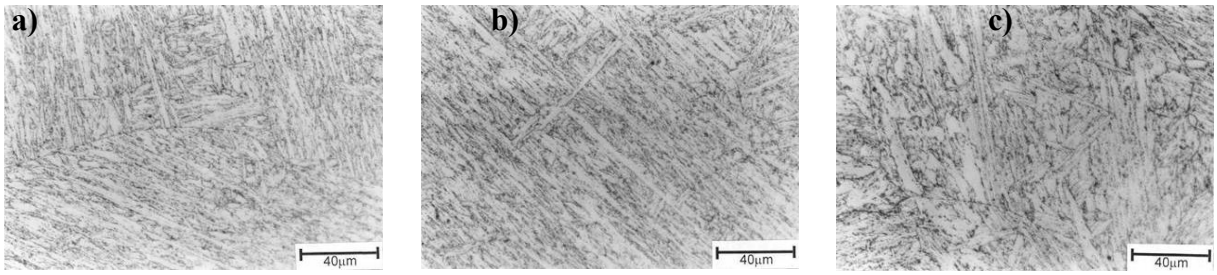

Fig. 6 Comparison of the optical micrographs as crept.
a) Alloy A, 145MPa @ 650°C, 430hr
b) Alloy B, 131MPa @ 650°C, 2133hr
c) Alloy C, 152MPa @ 650°C, 989hr

The promising creep behavior of steels would be attributed to the microstructure features and their stabilities under the influence of temperature and stress. In general, the microstructure of the alloys A, B and C in the quality heat treated condition consisted of tempered martensite and precipitates. Fig. 7 shows representative TEM image for the crept specimens at 600°C of the alloys A, B and C. These materials exhibit different substructure with subgrain and laths. In the alloy A, the subgrain was found after crept at 360hrs. However, the subgrain could not find out after crept more than 2200 hrs in alloy B and C. Martensite laths were decorated with $M_{23}C_6$ and were stabilized by $M_{23}C_6$ carbides which represented the dominant particle type within alloy B and C containing Mo and W.

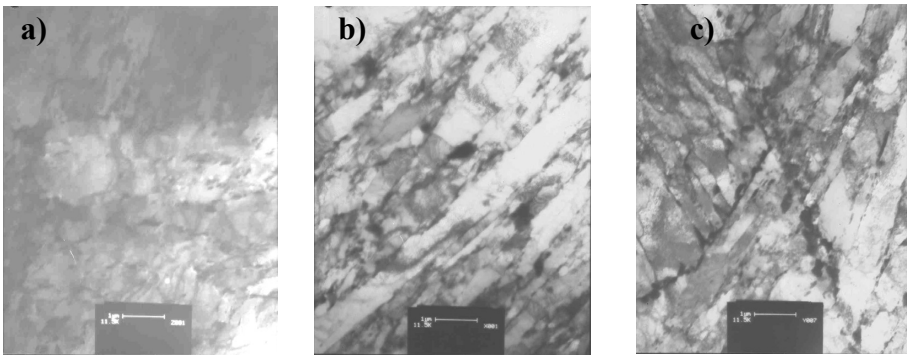

Fig. 7 Comparison of the TEM micrographs as crept.
a) Alloy A, 250MPa @600°C, 362 hr
b) Alloy B, 250MPa @600°C, 2230 hr.
c) Alloy C, 250MPa @600°C, 2520 hr.

Fig. 8 shows X-ray diffraction profiles for the extracted residues after crept of alloys A, B and C. The peak detected in alloy A was identified as $M_{23}C_6$ and MX. On the other hand, the peak detected in alloy B and C indicated Laves phase besides $M_{23}C_6$ and MX. It is likely that the formation of Laves phase(Fe_2Mo or Fe_2W) resulted from Mo and W content in comparison with alloy A (Fig.8 b) and c)). The addition of W and Mo in 9~12%Cr steel has a tendency to form Laves phase. Alloy A, B and C indicated $M_{23}C_6$ as the main peak and MX as the minor peak. The Laves phase peak of alloy C was higher than that of alloy B. These coincided well with results of creep behaviour and TEM observation. From these results, alloy C was selected into HIP rotor material for 600°C class USC power plant.

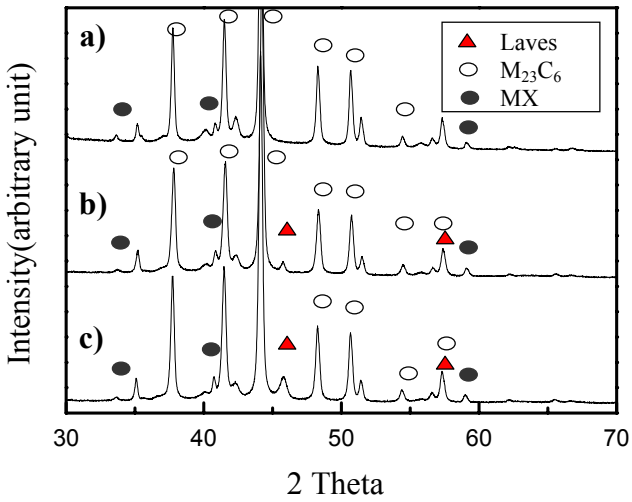

Fig. 8 XRD profiles of the residues extracted from the as crept specimen.
a) Alloy A, 250MPa @600°C, 362 hr
b) Alloy B, 250MPa @600°C, 2230 hr.
c) Alloy C, 250MPa @600°C, 2520 hr.

TRIAL ROTOR FORGINS PRODUCTION

Based on the test results described before, trial HIP turbine rotor was manufactured and subjected to verification testing. The manufacturing processes are shown in Fig. 9. This steel was refined by electro slag remelting(ESR) process to ensure a uniform chemical composition. The ESR ingot of diameter in 1000mm was manufactured from an electrode of 800mm diameter after steel refining by basic electric arc furnace(EAF).Because of the homogeneous structure and pipe free solidification of the ESR ingot, the forging process might be simple comparing with conventional ingot. The upset ingot was then forged to an intermediate size and followed by cogging.

The forging process was immediately followed by a preliminary heat treatment. After austenitizing, the rotor forging was subjected transformation in order to improve its machantability and ultrasonic attenuation. The preliminary heat treatment ensured a sufficiently finely grained structure, which was further improved by subsequent quality heat treatment. Quality heat treatment of austenitizing at 1050^{o}C and oil quenching and subsequent double tempering were executed. The trial rotor forging is shown in Fig. 10.

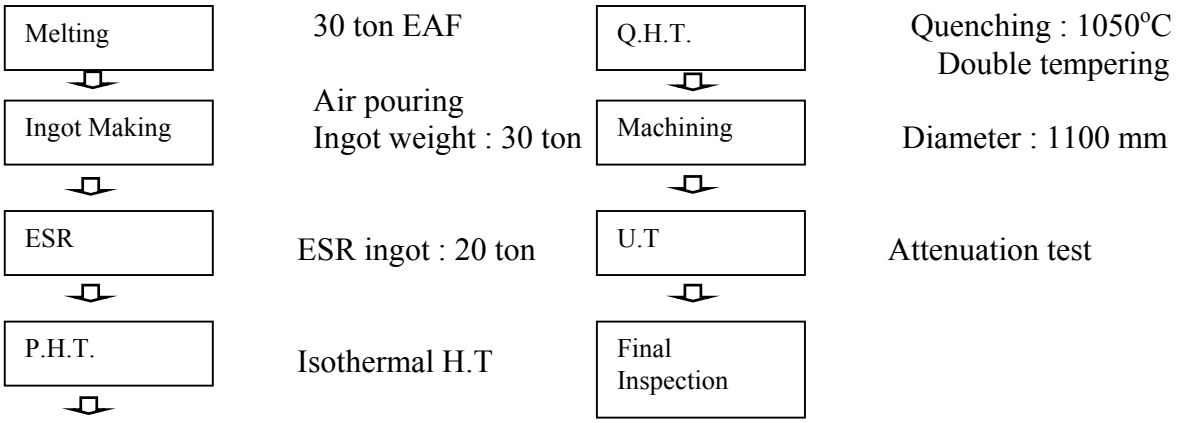

Fig. 9 Manufacturing process of trial rotor forging.

Fig. 10 Trial rotor forgings

MELTING OF ESR INGOT

The ESR electrode of 20 ton was manufactured by a 30ton EAF and ladle refining furnace. Selected raw materials were melted in the EAF to a low phosphorous content heat and the molten steel was tapped without Si and Al alloy addition. Before reduction refining in the ladle furnace, deslagging of EAF slag was carried out to minimize the increase of phosphorous content and then replaced with a synthetic basic slag. In the ladle furnace, fine correction of the melt chemistry and temperature was performed and degassed to control the low hydrogen and sulfur content.

ESR was carried out under inert atmosphere to prevent the re-oxidation of the oxygen-affine elements in the electrode and the hydrogen absorption from the air. ESR slag composition containing some SiO_2 was selected on the base of pilot ESR experiment to obtain the optimum Si, Nb and a low Al content. The melt rate was kept low and stable as much as possible. The metal samples were taken from the axial surface, middle and center of the product to check the behaviour of the main elements such as Cr, Si, Al and Nb content. Slag for chemical analysis was taken at the start of remelting and at the end of hot topping to predict the chemical composition of the product.

Table 2 shows the aim of electrode chemical composition of the ESR ingot for 20 ton trial rotor. The analysis result of oxides in slag and the behaviour of Si, Al, Nb, and the Cr contents in ingot are shown in Table 3 and Fig.11 respectively. As shown in the Table 3 and Fig.11, SiO_2 content increased from 3.3 to 4.7%. Although Si, Nb and Cr contents in the bottom section were a little less than that in the other section, the contents of all elements satisfied with target range.

Table 2 The aim chemical composition of electrode(wt%).

	C	Si	Mn	Ni	Cr	Mo	V	Al	Nb	W	N
Min.	0.10		0.40	0.60	10.00	1.00	0.15		0.040	0.95	0.040
Max.	0.15	0.10	0.60	0.80	10.60	1.20	0.25	0.015	0.070	1.10	0.070

Table 3 Chemical composition change of ESR slag(wt%).

Process	SiO_2	Total Fe	MnO
Before ESR	3.3	0.03	0.03
After ESR	4.7	0.15	0.3

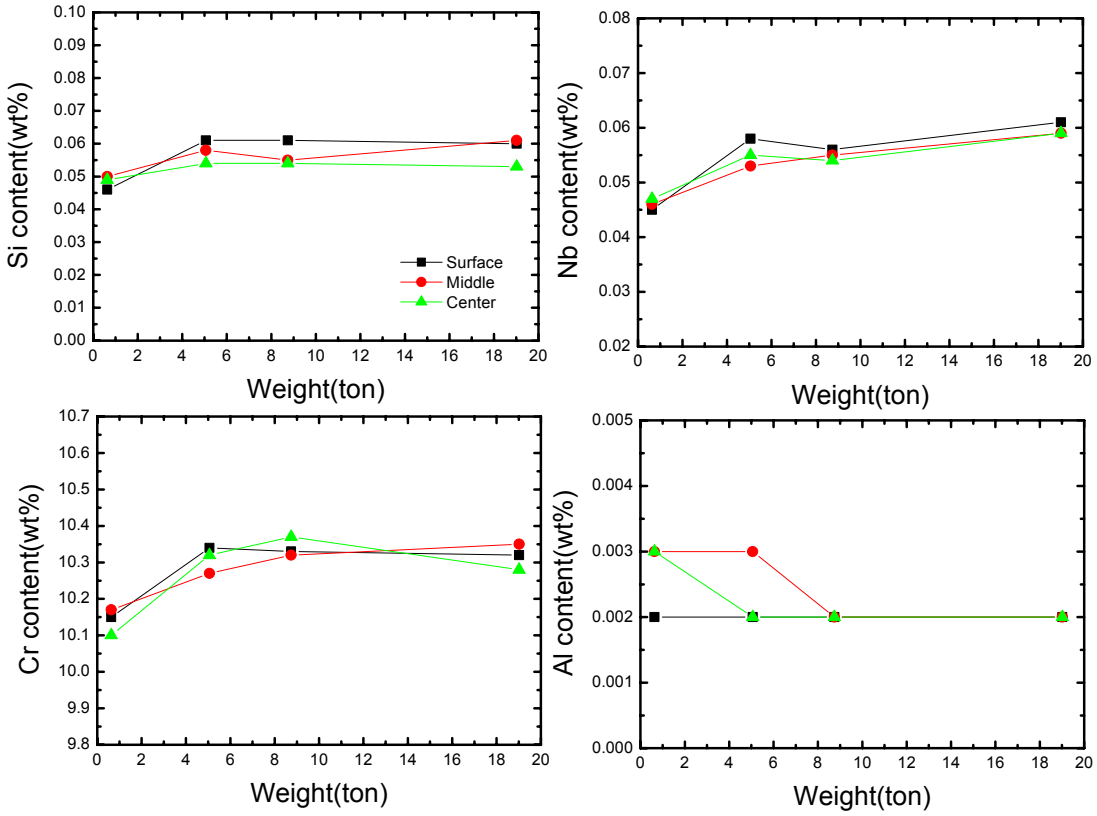

Fig. 11 Chemical composition of 20ton ESR ingot.

The behaviour of Si, Cr and Nb in the bottom portion was unstable. These might be resulted from an imperfect inert gas control at the start of remelting. The oxygen within the mould may preferentially react with the Si of the electrode and form SiO_2, which in turn would be absorbed by the slag. So, Si content of ingot decreased and SiO_2 activity in slag also increased. As the SiO_2 activity in slag increases, Nb and Cr content will decrease.

FORGING AND HEAT TREATMENT

The ingots were double upset forged with 4200 MN press. Forging parameters such as temperature, soaking time and deformation rate were important to ensure the prevention against forging defect and suitable microstructure. To optimise the forging sequence and to improve the reproducibility of the forging process, the forging process on the basis of FEM modelling was designed. Fig. 12 shows the simulation result of upsetting process.

In order to allow the ultrasonic test of the forgings in the quality heat treatment condition, the optimum preliminary heat treatment was to be applied. Transformation of the full ferrite phase provided a good condition for ultrasonic test. After rough machining, the quality heat treatment was performed by austenitizing at 1050^{o}C followed by double tempering at different temperature.

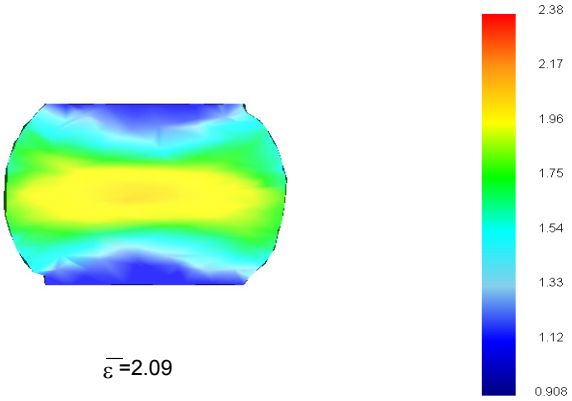

Fig. 12 Distribution of the effective strain during upsetting.

MATERIAL EVALUATION

The test pieces taken from the trial rotor are shown in Fig 13. Product analysis results are presented in Table 4. The chemical composition is very homogeneous.

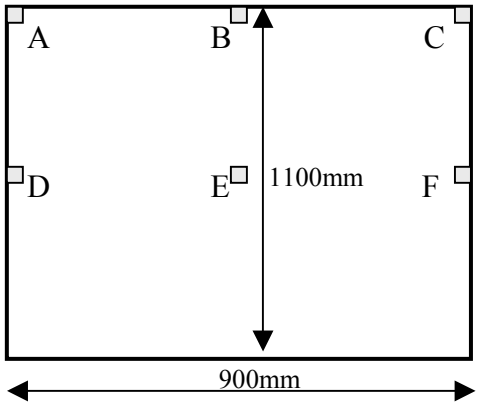

Fig. 13 Test block of trial rotor in dimension and specimen location.

Table 4 Chemical composition(wt%) of the trial rotor forgings at various locations.

Sample location		C	Si	Mn	P	S	Ni	Cr	Mo	V	Nb	W
Ladle		0.12	0.07	0.52	0.006	0.002	0.75	10.20	1.09	0.20	0.060	1.02
Surface	A	0.12	0.05	0.50	0.004	0.001	0.74	10.23	1.09	0.19	0.052	1.02
	B	0.13	0.05	0.50	0.006	0.001	0.74	10.24	1.05	0.19	0.054	1.05
	C	0.13	0.04	0.50	0.008	0.001	0.73	10.15	1.04	0.18	0.047	1.03
Center	D	0.13	0.06	0.52	0.003	0.004	0.73	10.17	1.09	0.19	0.056	1.02
	E	0.13	0.03	0.50	0.005	0.001	0.74	10.14	1.05	0.19	0.050	1.05
	F	0.14	0.04	0.44	0.009	0.001	0.72	10.13	1.04	0.17	0.046	1.00

Fig. 14 shows the macrostructure for block taken from the longitudinal and transversal direction after heat treatment. Neither distinct segregation and cavity, nor other harmful imperfections are observed.

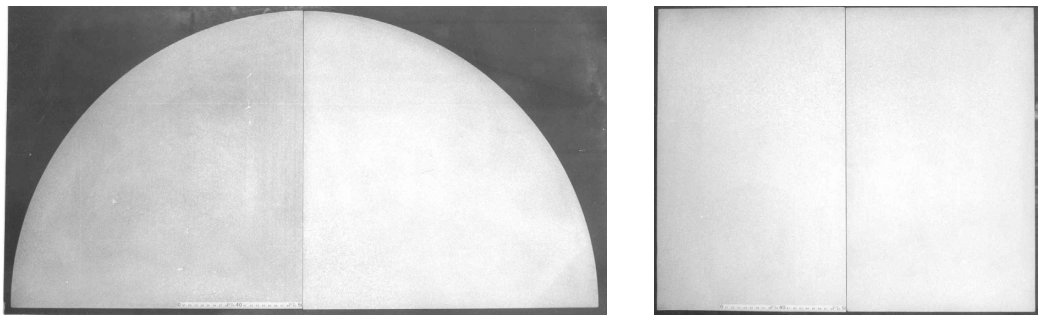

Fig. 14 Macrostructure of cross section and longitudinal direction.

The mechanical properties were tested at three locations. Specimens were taken in the radial and longitudinal directions at surface of rotor and also in the radial direction at the body center. The results of basic strength and toughness properties are summarised in Table 5. Table 5 shows the tensile and Charpy V-notch impact properties at surface and center of the rotor forgings. The obtained results have sufficient margin in comparison with target values. The difference in tensile strength between the surface and the center was small, and excellent toughness was also obtained.

Table 5 Mechanical properties of the trial production rotor forgings at various locations.

Location	0.2%Y.S (MPa)	T.S (MPa)	EL (%)	RA (%)	E_{impact} (J)	FATT (^{o}C)
Target	>723	827~965	>13	>40	>27	< 52
B, Radial	782	892	22	63	75	22
B, Longi.	790	899	22	63	65	25
E, Radial	773	882	21	61	56	22

The microstructure from surface to center of the rotor forgings was tempered martensite with a grain size of ASTM No in 3 ~ 4 as shown in Fig. 15. A tempered martensite structure was observed across all regions of the rotor. No delta ferrite was observed, this result was due to the Cr equivalent of a below 10.

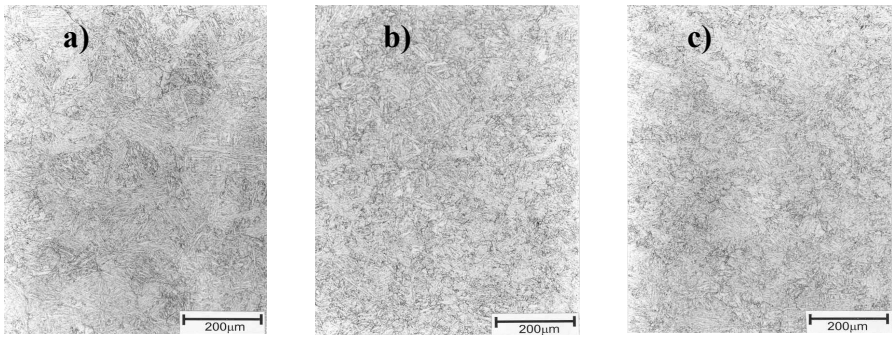

Fig. 15 Optical micrographs of trial rotor at various locations.
a) Surface b) Middle c) Center

Ultrasonic examination was done on the machined rotor. No defects could be found. Detectable flaw size was less than 1.0mm in size for diameter 1100mm.

In addition, short term creep tests at 600°C were performed to meet the requirement. 10^5hrs Creep rupture strength at 600°C is higher than 100 MPa as shown in Fig. 16. Further long term test is ongoing. The trial rotor forging was remarkably homogenous from top to bottom as well as from surface to center.

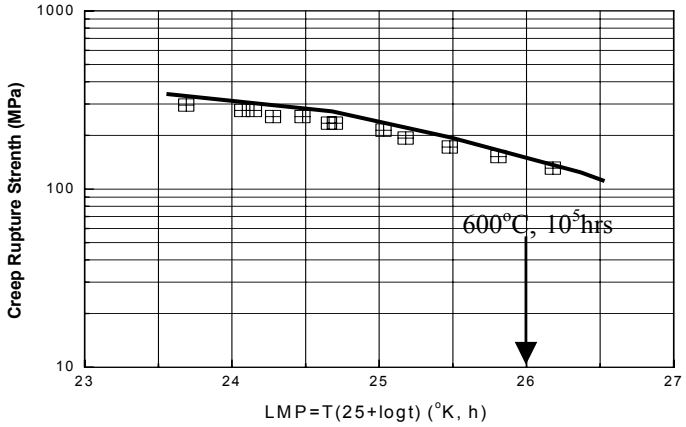

Fig. 16 Creep rupture strength of trial rotor.

CONCLUSION

In order to develop rotor material of superior creep resistance for fossil power plants, Alloy C steel was selected as a optimal composition on the basis of tests performed by Doosan heavy industries, Ltd. Accordingly, trial rotor forgings was produced. The research results obtained could be summarized as follows.

1) Based on fundamental investigation, 10CrMoVNbN steel containing 1% W might be an optimum chemistry as the HIP rotor steel of 600°C class USC power plant.

2) The trial rotor forging of 1100mm in diameter was successfully manufactured from a diameter of 1000mm ESR ingot.

3) The microstructure at various locations showed a fine tempered martensite. No differential was observed with respect to the mechanical properties at surface and center of rotor forgings.

4) Homogeneous metallurgical and mechanical properties in the whole forgings were confirmed.

REFERENCES

1) V. K. Sikka, M. G. Gowgill and B. W. Roberts, Proc. Conf. Ferrite alloys for use in nuclear energy technology, Snowbird, Utah(1983)
2) Y. Nakabayashi et al., Proc. of 1st EPRI Int. Conf. ICPP, Palo Alto(1986)
3) K.H. Mayer, R. Blum, P. Hillenbrand, T. U. Kern and M. Staubli, 7th Liege COST Conf. Liege, Belgium(1994)
4) B. Scarlin, T. U. Kern and M. Staubli, Proc. of 4th EPRI Int. Conf. Advances in Materials Technology for fossil Power Plants, South Carolina(2004)
5) T. Tcuchiyama, O. Matsumoto, O. Ishiyama, Y. Yasumoto and T. Abe, Proc. Conf. Advanced Heat Resistant Steels for power Generation, San Sebastian(1988)
6) D. V. Thornton and K. H. Mayer, Proc. Conf. Advanced Heat Resistant Steels for power Generation, San Sebastian(1988)
7) M. Miyazaki, M. Yamada, Y. Tsuda and R. Ishi, Proc. Conf. Advanced Heat Resistant Steels for power Generation, San Sebastian(1988)
8) Y. Tsuda, M. Yamada, R. Ishii, Y. Tanaka, T. Azuma and Y. Ikeda, Proc. 13th, Int. Forgemasters Meeting, Busan(1997)
9) T. Kern et.al., Proc. 15th, Int. Forgemasters Meeting, Kobe(2003)
10) S.H. Ryu, M.S. Kim, Y.S. Lee, J.T. Kim, J. Yu, and B.J. Lee, 4th Int. Conf. on Advances in Materials Technology for Fossil Power Plants, South Carolina (2004)
11) S.H. Ryu, Y.S. Lee, B.O. Kong, and J.T. Kim, Proc. of First Int. Conf. on Advanced Structural Steels (ICASS 2002), Tsukuba(2002)
12) S. H. Ryu et al., Proc. of the 5th Int. Charles Parsons Turbine Conf., Cambridge(2000)

HOME